CORRELATING NEAR-SOURCE ROCK DAMAGE FROM SINGLE-HOLE EXPLOSIONS TO SEISMIC WAVES

Randolph Martin[1], Peter Boyd[1], Anastasia Stroujkova[2], Mark Leidig[2], James Lewkowicz[2], and Jessie Bonner[2]

New England Research Inc.[1] and Weston Geophysical Corporation[2]

Sponsored by the Air Force Research Laboratory

Award No. FA9453-10-C-0257
Proposal No. BAA10-19

ABSTRACT

Weston Geophysical Corporation (WGC) and New England Research, Inc. (NER) conducted the New England Damage Experiment (NEDE) in July 2008. The experiment included the detonation of five small (135 to 270 lbs) chemical explosions in relatively unfractured, homogeneous Barre granite in Vermont, USA. Barre granite has been a worldwide standard for homogeneous, low fracture-density granite in commercial, monument, and industrial settings. The emplacement granite was characterized before and after the experiment using borehole cores and acoustic imaging. The explosions were designed with variable velocities of detonations (VOD) to fracture the rock differently. Our hypothesis was that different damage would lead to possible variations in *S*-wave generation. During the past year, we have quantified the damage from the explosions on micro, meso, and macro scales and examined the seismic wave generation and propagation at near-source, local, and regional distances.

Pre-shot site characterization indicates that although the Barre granite is massive with a low fracture density, it is transversely isotropic. The anisotropy is largely due to the rift, a planar array of microcracks. The elastic anisotropy is on the order of 20%. After the five shots were detonated, a coring program was undertaken to determine the subsurface characteristics of the damage generated by each detonation at various distances from each shot point. The pre-shot cores were recovered with few pre-existing fractures. In contrast, the post-shot cores show extensive damage. The intensity of the damage decreases with range.

The large scale and microscale damage of each core were studied. Based on the degree of damage, five distinct zones were identified. The damage ranged from highly pulverized/granulated rock with possible cavity development through intact rock with high angle fractures parallel to the rift above the emplacement level to mostly intact with few fractures that are generally randomly oriented. The shapes of damage zones are non-spherical with lateral extension at the emplacement depth of the charge. Microscale damage is concentrated in the horizontal plane at the emplacement depth and a vertical ellipsoid through the working point. There is little off axis microscale damage resulting in a decidedly non-spherical damage surface.

We studied seismic wave generation from the five NEDE explosions. The near-field (< 20 m) accelerations exceeded *g* for the ANFO and COMP-B shots, indicating the rock mass above the explosion was lifted without breaking and released the elastic energy during spall. In contrast, the Black Powder produced acceleration slower than *g*, perhaps due to breaking the entire rock layer above the shot. Large ground fractures, permanent uplift, and large amplitude surface waves produced by Shot 1 support this conclusion. We analyzed empirical scaling relationships for different phases at multiple distance ranges using spectral ratios. The COMP-B shots produced larger *P*-wave amplitudes and smaller Love wave amplitudes than equivalent yield ANFO and Black Powder shots. We observed complex non-uniform amplitudes for short-period Rayleigh (*Rg*) waves generated from the NEDE shots. At frequencies above 5 Hz, the COMP-B shots typically have similar or larger *Rg* amplitudes when compared to equivalent yield ANFO and Black Powder shots. Amplitudes for *Lg* at local-to-regional distances mimic the *Rg* behavior, which may have important implications for *S*-wave generation.

OBJECTIVES

Shear wave generation from explosions continues to be an important problem for the nuclear explosion monitoring community. Damage from the explosion may also play an important role in shaping the seismic waves from an explosion. Most recently, Patton and Taylor (2011) have demonstrated the importance of considering the moment from the damage separate from the explosion moment. Additional proposed mechanisms of explosion-generated *S*- waves involve processes related to the damage and deformations caused by the explosions. Nonlinear effects in the immediate vicinity of the explosion cause rock damage that can effectively generate shear-waves provided that asymmetries exist in the damage pattern (Ashby and Sammis, 2000). Sammis (2003) has suggested that movement along pre-existing cracks can also produce large amplitude *S*-waves. Bykovtsev (2007) has postulated that radial crack generation from explosions should generate *S*-waves with distinct radiation patterns.

WGC and NER conducted the NEDE in July 2008. The experiment included the detonation of five small (135 to 270 lbs) chemical explosions in relatively unfractured, homogeneous Barre granite in Vermont, USA. Barre granite has been a worldwide standard for homogeneous, low fracture-density granite in commercial, monument, and industrial settings. The emplacement granite was characterized before and after the experiment using borehole cores and acoustic imaging. The explosions were designed with variable VODs to fracture the rock differently. The objective of this report is to provide a model for the macro-, meso-, and micro-damage from the NEDE explosions.

RESEARCH ACCOMPLISHED

Damage Analysis: Pre-Shot Studies

Test Site Geology. The Barre Granite at the NEDE test site was selected for the study because it is a monument grade rock mass with a low fracture density. A prominent feature of Barre Granite is the rift, or nearly vertical planar feature that strikes at N30°E at the test site. The rift is defined by a set of pervasive, similarly oriented, open and partially healed, inter- and intra-granular microcracks (Nasseri and Mohanty, 2008). Visible fractures were observed on quarry faces with spacing on the order of 4 to 5 m. The fractures are typically clean, planar sub horizontal features, which represent sheeting joints that follow the topography (Richter, 1987). The homogeneity was verified with a ground penetrating radar (GPR) study of the site and a borehole geophysical logging program using an oriented acoustic televiewer, an optical televiewer, and a caliper. In addition, detailed observations on two pre-shot coreholes verify the low fracture density. The site is above the water table; no water infiltrated the emplacement holes for the explosives.

To quantify the damage to the granite resulting from the explosions, the physical properties of the granite were measured from cores recovered from holes drilled before the detonations. Two control holes were cored adjacent to the emplacement holes for Shots #2 and #5, as shown in Figure 1. There was complete core recovery from the pre-shot coreholes.

Rock Properties. A comprehensive suite of laboratory scale measurements was performed on the core to determine the properties of the site in the pre-shot condition. The measurements included:

- Bulk properties,
- Diametral *P* and *S*-wave velocities along the axis of the core recovered from coreholes,
- Compressional and shear wave velocities as a function of pressure,
- Linear compressibility as a function of pressure,
- Fluid permeability as a function of pressure,
- Electrical resistivity as a function of pressure, and
- Rock strength.

The *P* and *S*-wave velocities were measured on the cores as a function of depth and azimuth at ambient conditions. Time of flight velocity measurements were performed along the core in a bench top apparatus. At each point, the core was rotated between the transducers. The velocity varied with azimuth. A typical data set collected with the bench top setup is shown in Figure 2. Velocity increases from a minimum value of 3.84 km/sec to a maximum value of 4.56 km/sec as the core was rotated 90° from the minimum value. The two pre-shot cores were evaluated in this

way and the location of the rift was marked on the surface of the core. This facilitated sub-coring for subsequent experiments at pressure.

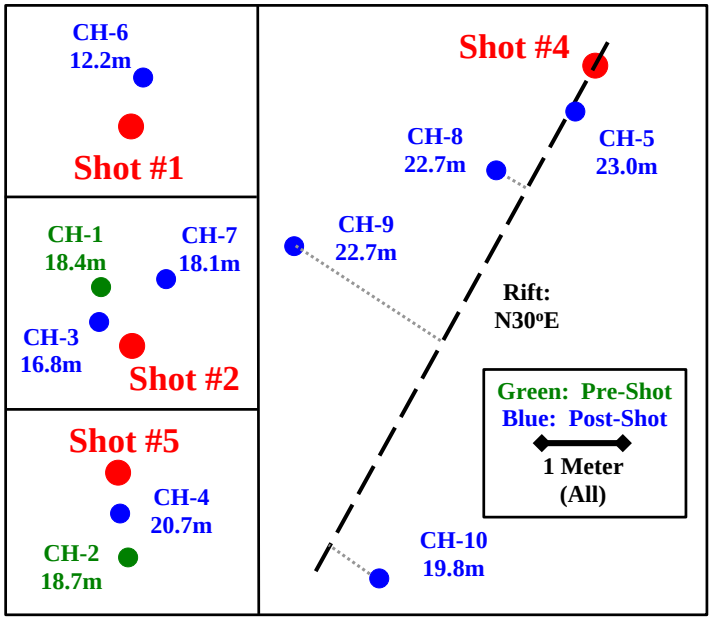

Figure 1. Location of coreholes and depths near the NEDE shots. Core diameter is nominally 51 mm.

Figure 3 shows the velocity data parallel and normal to the rift as a function of depth for the core recovered from CH-2. Note that there is scatter in the velocity and a gradual increase with depth. A least squares fit to the data for each orientation was calculated. The axis of the colored cloud for each orientation is parallel to the fit.

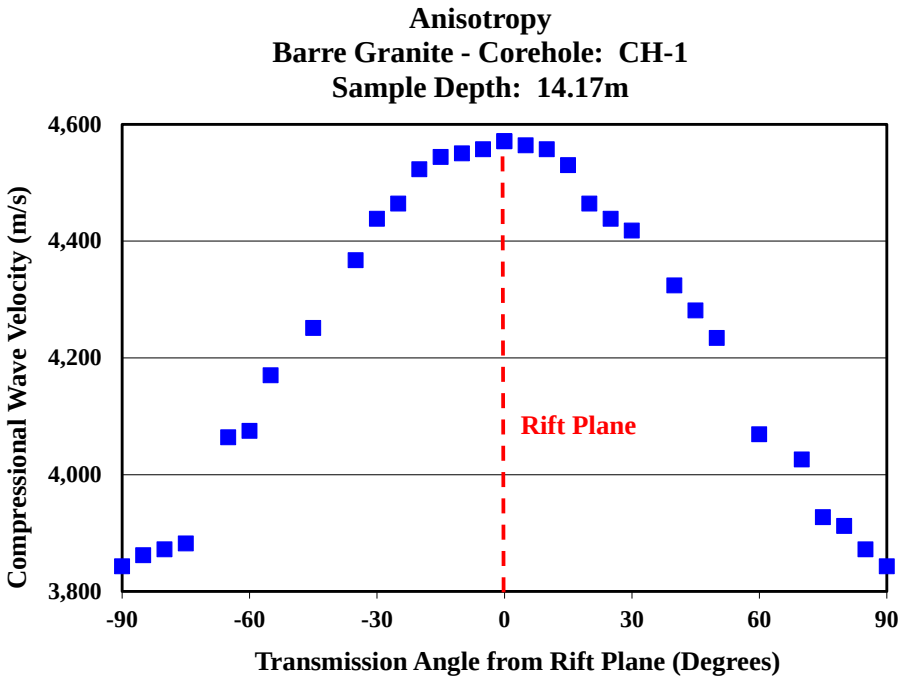

Figure 2. Compressional wave velocity anisotropy measured in the Barre granite.

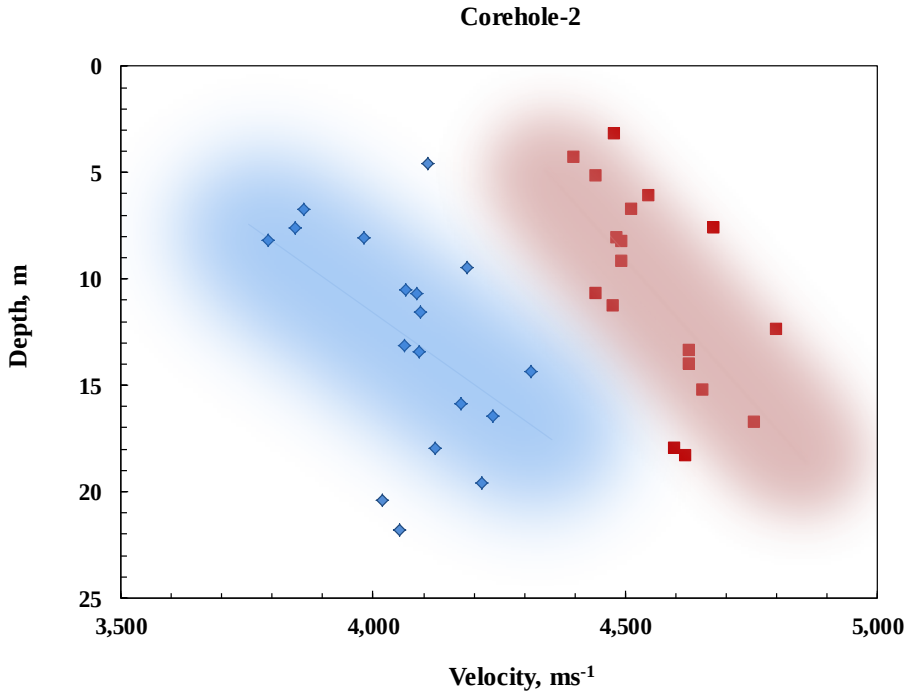

Figure 3. Fast (red) and slow (blue) velocities for Barre granite core samples as a function of depth below the surface.

To further evaluate the anisotropy associated with the rift, oriented sub-cores 38 mm in diameter and 38 mm in length were cut parallel and normal to the rift. Measurements of compressional and shear wave velocity, electrical resisitivity, and permeability were performed as a function of pressure. The initial velocities were 3.325 km/sec normal to the rift and 4.205 km/sec parallel to the rift. With increasing pressure the velocities increased; the rate of increase was greater for propagation perpendicular to the rift. The initial elastic anisotropy of 21% decreased to 5.5% at a pressure of 70 MPa. Presumably, if the test were carried out to pressures of several hundred MPa, most of the micro cracks would close and the velocities would asymptotically approach the same value. The samples were then saturated with a weak brine and measurements of permeability and electrical resistivity were carried out as a function of pressure. The initial permeability anisotropy decreased from 27% to near zero with a moderate increase in pressure. The resistivity anisotropy did not exhibit the strong pressure dependence observed for velocity and permeability. Although the resistivity for both orientations increased three-fold with pressurization to 50 MPa, the anisotropy remained more or less constant at 26 to 28%. These data are consistent with many previous studies on granite.

Damage Analysis: Post-Shot Studies

After the five shots were detonated, a comprehensive study was undertaken to examine the damage generated in the vicinity of each core hole. Of particular interest are the types of damage that occurred and the extent of the damage laterally and vertically away from the working point. Blast induced damage can be characterized at three scales: macro (distinct, singular fractures at hand specimen/core scale), meso (highly fragmented to granulated zones with indistinct fracture planes), and micro (microscopic). Larger scale damage is present at all shot locations, but microscale damage is only observed at the higher VOD (ANFO and COMP-B) shots.

There was little surface expression due to the explosions. Surface fractures were observed at the black powder and the two ANFO shots; none were observed in the vicinity of the COMP-B shots. To further characterize changes in the vicinity around each shot point, a GPR study was initiated. The goal of the study was to look for new fractures that developed due to the explosions and to examine the extent of fracturing away from the shot point. These studies

proved inconclusive. They were unable to delineate fragmentation or new fractures that developed in the vicinity of each shot point. However, the GPR survey verified that the site was homogeneous.

A detailed coring program was undertaken to determine the subsurface characteristics of the damage generated by each detonation. Eight coreholes were drilled at various distances from each shot point. Figure 1 gives the location of the coreholes with respect to the shot points. The depths of the coreholes ranged from 19.8 to 23 m. The pre-shot cores were recovered with few pre-existing fractures. In contrast, the post-shot cores show extensive damage. The intensity of the damage decreases with range from the blast point. Importantly, the core collected adjacent to Shot #1, the black powder shot, showed no microscale damage. This shot also produced the greatest shear wave amplitudes.

In order to quantify the radial and vertical extent of the damage, Shot #4, a 270 lb ANFO detonation, was selected for detailed study in 2010. Four boreholes were drilled approximately along the trend of the rift from the working point to a range of 7.01 m as shown in Figure 1. The large scale and microscale damage of each core were studied. Figure 4 presents a schematic interpretation of these data. The geometries of the distinct damage regions are complex. The most accurately defined are the microscale features. Of particular note is that no macroscale fracturing extends below the explosive charge, but it extends laterally at least beyond the farthest borehole. The free surface and confinement with depth below the blast control this result.

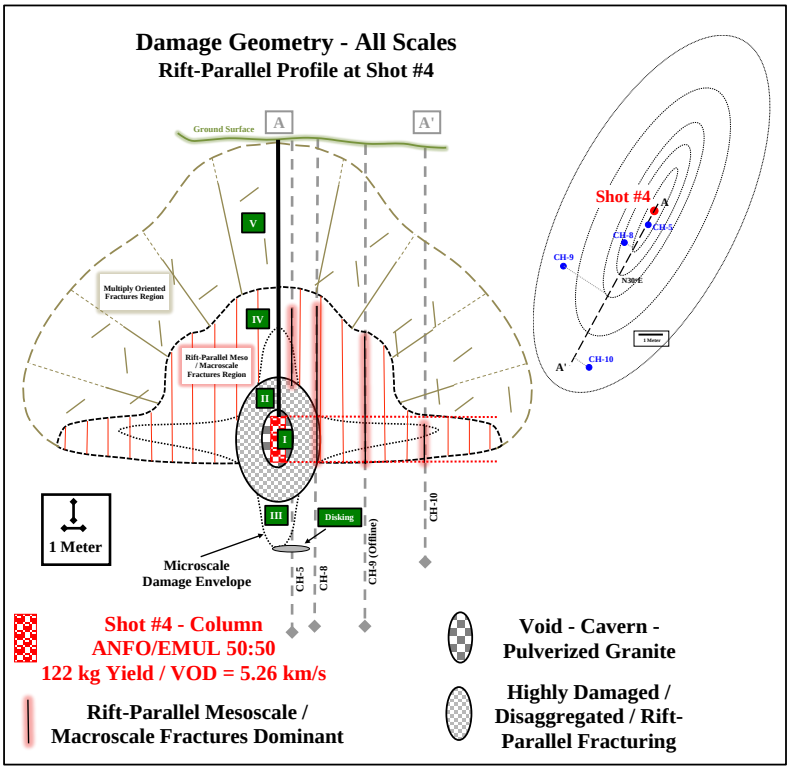

Figure 4. Schematic cross section at Shot #4 showing the distribution of damage of all scales. Distinct damage regions are identified. The non-spherical geometry of damage is evident. The elliptical representation of the lateral damage in plan view cannot be confirmed with the available data, but is presented as a working hypothesis.

We identified five distinct zones based on the degree of rock damage, which are delineated in Figure 4. Examples of core specimens from each zone along with a brief description of the rock fragments are presented in Figure 5. A more detailed analysis of the character of the damage of each zone is currently under way. A preliminary assessment of the data yields a damage surface that is non-spherical. Similar findings were also seen for a limited number of cores recovered adjacent to the 135 lb ANFO shot and the 270 lb COMP B shot.

The distinct damage zones include:

- ***Damage Region I*:** Highly pulverized/granulated with cavity development possible. Microscale damage is extreme**.**
- ***Damage Region II*:** Significant disaggregation with numerous high angle fractures that strike parallel to the rift. Extreme microscale damage is also evident in intact core pieces. Damage extends above and below explosives emplacement level.
- ***Damage Region III***: Generally intact. Extent of region determined with acoustic velocity measurements; the microscale damage greatest nearer to shot point. Core can take on a "milky" appearance due to the microscale damage. High angle fractures parallel to the rift present in only the portion of region above the emplacement level.
- ***Damage Region IV*:** Generally intact with few high angle fractures that are all parallel to the rift. Microscale damage only exists close to the working point.
- ***Damage Region V*:** Mostly intact with few fractures that are generally randomly oriented. Large scale fracturing extends to the surface at the Black Powder and ANFO/Emulsion shots. Microscale damage is not present.
- ***Core Disking Feature*:** Core disking was encountered in three coreholes. It was most prevalent at Shot #5 in CH-4, and in all cases is located within or very near the explosives column level. Disking is created by the action of the coring operation and is attributable to residual horizontal stress at depth. In this case, the stresses may have been induced by the blasts**.**

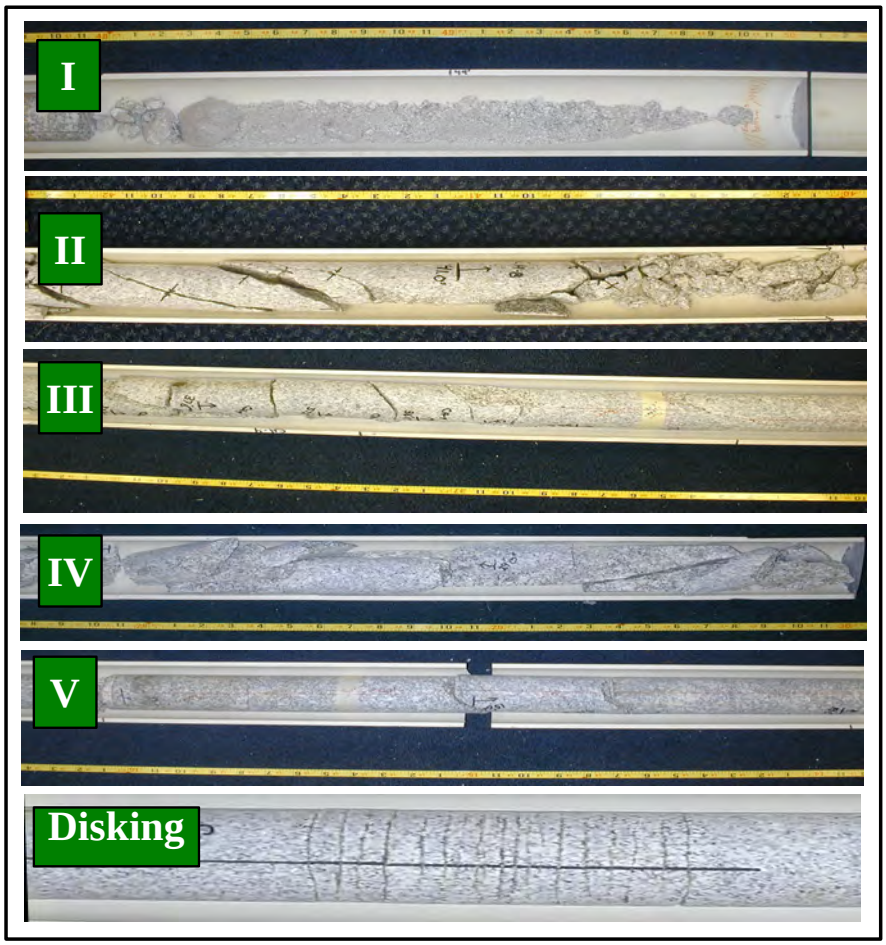

Figure 5. Examples of damage regions outlined in Figure 4. The damage is transitional in intensity and in mode of formation.

On many of the pieces of core the orientation of fractures is parallel to the rift. This suggests that the rift at the site controls not only the elastic properties, but also the mechanical properties. To study this effect, a confined compression experiment was carried out on a cylindrical sample with its axis parallel to the core hole. The rift was identified and the specimen was instrumented to monitor strain parallel and normal to the rift, and parallel to the loading axis. In addition, compressional and polarized shear waves were propagated parallel to the core axis. The shear wave polarizations were oriented parallel and normal to the rift. The sample compacted to approximately half the compressive strength and then began to dilate, that is cracks began to open parallel to the loading axis. The transverse strains did not increase equally. The transverse strain normal to the rift increased more rapidly than the transverse strain in the rift plane. The difference persisted until the sample failed. At failure, the strike of the fracture plane was parallel to the rift.

The shear velocities increased up to approximately half the compressive strength, remained more or less constant to three quarters of the strength, and then decreased continuously until the rock failed. For the shear wave polarization in the rift, velocities increased more than that normal to the rift as shown in Figure 6. As the sample began to dilate, the velocity and Q for the vibration direction normal to the rift decreased with respect to waves vibrating parallel to the rift.

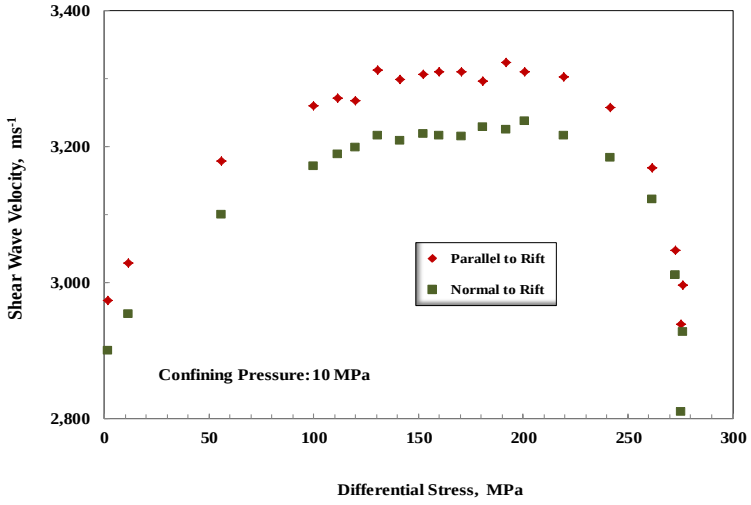

Figure 6. The effect of differential stress on shear-wave velocity in a Barre granite sample loaded to failure in confined compression.

Microscale damage is quantifiable and can be accurately delineated at the site. An earlier investigation on HARDHAT (Short, 1966) also reported blast induced microscale damage. For NEDE, each core was photographed and then bench top *P* and *S* wave velocity measurements were carried out on the intact sections and pieces of core to infer the magnitude of the microscale damage with depth and azimuth. Figure 7 shows the *P* and *S* wave velocities as a function of depth for a core recovered adjacent to Shot #5. The emplacement zone for the explosive is shown. The compressional and shear wave velocities decrease by 15 to 20% compared to the pre-shot values over a 5 m interval centered on the working point. Similar effects were observed in other post-shot coreholes adjacent to the high VOD Shots #2 and #4, but were not observed at the low VOD Shot #1.

As shown in Figure 1, four coreholes were drilled near Shot #4. The locations of the coreholes were selected to investigate the extent of damage outward from the blast parallel to the rift strike (N30^{o}E). Each new corehole position was based on the extent of damage (slowing of the compressional wave velocity due to microscale damage) observed in the previous one. The objective was to determine the boundary between the damaged (inelastic) zone and the elastic regime.

The velocity profiles shown in Figure 8 were analyzed to determine the boundary between the elastic and inelastic (damaged) regions. Moving outward from the working point of the blast the thickness of the damaged zone

decreases from 13 m to approximately 1 m at a range of 7.01 m. Presenting the section at equal scales leads to the interpretation shown in Figure 4 as Region III. The non-spherical nature of the damage is evident, and its reach is greater than had been predicted from previous studies.

The microcrack damaged interval is large near the shot, but narrows within a short distance from the shot and extends horizontally for several meters. The cross sectional shape of the microcrack damage zone was not what we expected (Figure 4). Based on the existing literature, we expected a more spherical shape for the transition to elastic behavior. Only the area SW of the shot point has been investigated thus far.

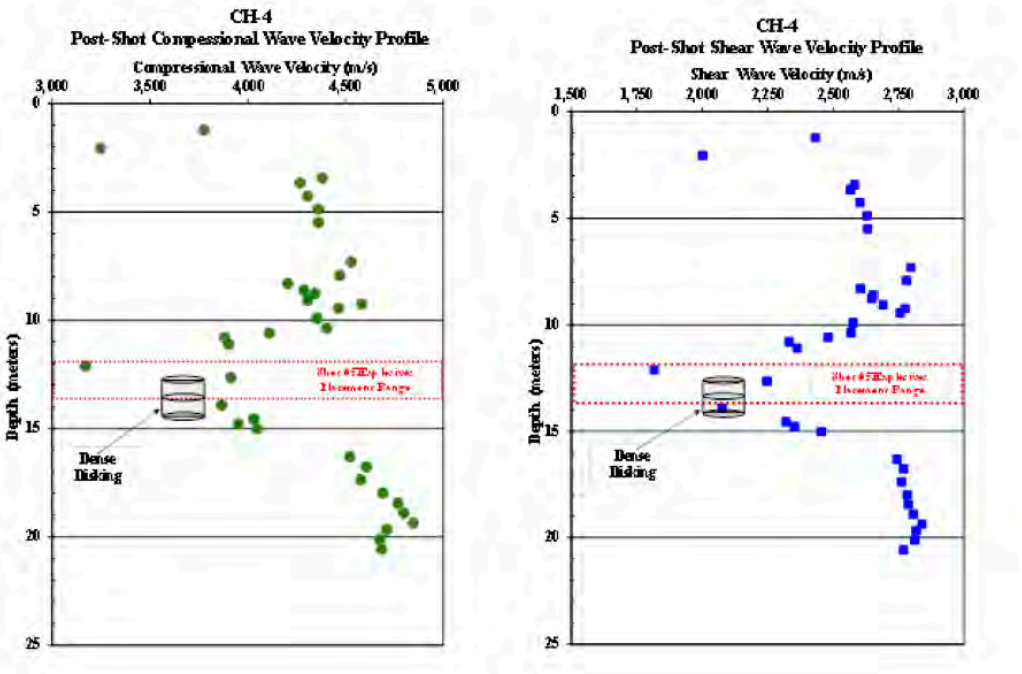

Figure 7. CH-4 *P* and *S* velocity profiles. The low velocity region reflects the microscale damage induced by the blast. Note that damage intensity increases with greater proximity to the explosive charge. The extent of this damaged zone scales with the yield of the blast.

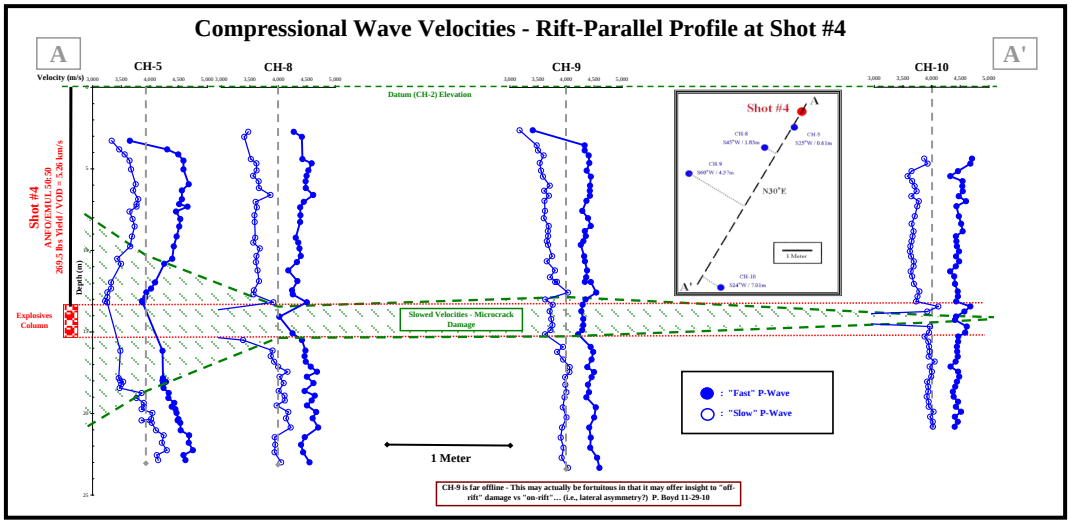

Figure 8. Cross section at Shot #4 with detailed velocity profiles. The horizontal scale is expanded. The location of coreholes is shown in upper right.

Seismic Analysis

We studied seismic wave generation from the NEDE explosions with the results summarized in Table 1. The explosions fractured rock differently, with radial cracks observed on the surface for the ANFO and Black Powder shots and none for the COMP-B shots. The near-field (< 20 m) accelerations exceeded *g* for the ANFO and COMP-B shots, indicating the rock mass above the explosion was lifted without breaking and releasing the elastic energy during spall. In contrast, the Black Powder shot produced acceleration less than *g*, perhaps due to breaking the entire rock layer above the shot. Large ground fractures, permanent uplift, and large amplitude surface waves produced by Shot 1 support this conclusion.

We analyzed empirical scaling relationships for different phases at multiple distance ranges using spectral ratios. The COMP-B shots produced larger *P*-wave amplitudes than equivalent yield (*W* in kg of total explosives) ANFO and Black Powder shots. This can be partially explained by applying TNT equivalence factors for ANFO (0.8*W*) and COMP-B (1.35*W*) and then modeling the shots using a Mueller-Murphy (1971) explosion source model.

We observed complex non-uniform amplitudes for short-period Rayleigh (*Rg*) waves generated from the NEDE shots (Figure 9). For three quadrants (NW, NE, SE), the ANFO and Black Powder shots generated larger amplitude *Rg* than the equivalent yield COMP-B shots between 1-5 Hz. The ANFO shots, particularly Shot 2, have a radiation null that reduces *Rg* amplitudes in the SW quadrant, and similar reduction is not observed for the Black Powder and COMP-B shots. At frequencies above 5 Hz, the COMP-B shots typically have similar or larger *Rg* amplitudes in most quadrants when compared to equivalent yield ANFO and Black Powder shots. The ANFO and Black Powder shots also generated larger amplitude Love waves (Figure 10) than the COMP-B shots. Amplitudes for *Lg* at local-to-regional distances (Figure 11) mimic the behavior of the local *Rg* phase which may have important implications for *S*-wave generation.

Table 1: Seismic Characteristics from the NEDE

Shot #	***Fractures***	***P wave***	***Rg wave***	***Love waves***	***Lg wave***
1 (61 kg of Black Powder)	Large radial fractures with permanent displacement	*P* waves are deficient in high frequencies (>10Hz)	1-10 Hz *Rg* is larger or equivalent to ANFO and Comp B shots	Larger than Shot 2 (ANFO) and Shot 3 (COMP B)	Local-to-regional *Lg* mimics the complex behavior of the *Rg* at local distances.
2 (61 kg of ANFO)	Surface fractures, no permanent displacement	Larger than Shot 1 (BP) especially at high frequencies, smaller than Shot 3 (COMP B)	Complex amplitude pattern, amplitude decrease in the SW quadrant	Larger than Shot 3 (COMP B), smaller than Shot 1 (BP)	
3 (61 kg of COMP B)	No surface fracturing	Larger than Shot 1 (BP) and Shot 2 (ANFO)	At low-frequencies *Rg* show decreased amplitudes in the SE quadrant	Smaller than Shot 1 (BP) and Shot 2 (ANFO)	
4 (122 kg of ANFO)	Surface fractures, no permanent displacement	Smaller than Shot 5 (COMP B)	Complex amplitude pattern, amplitude decrease in the SW quadrant	Larger than Shot 5 (COMP B)	
5 (122 kg of COMP B)	No surface fracturing	Larger than Shot 4 (ANFO)	At low-frequencies *Rg* show decreased amplitudes in the SE quadrant	Smaller than Shot 4 (ANFO)	

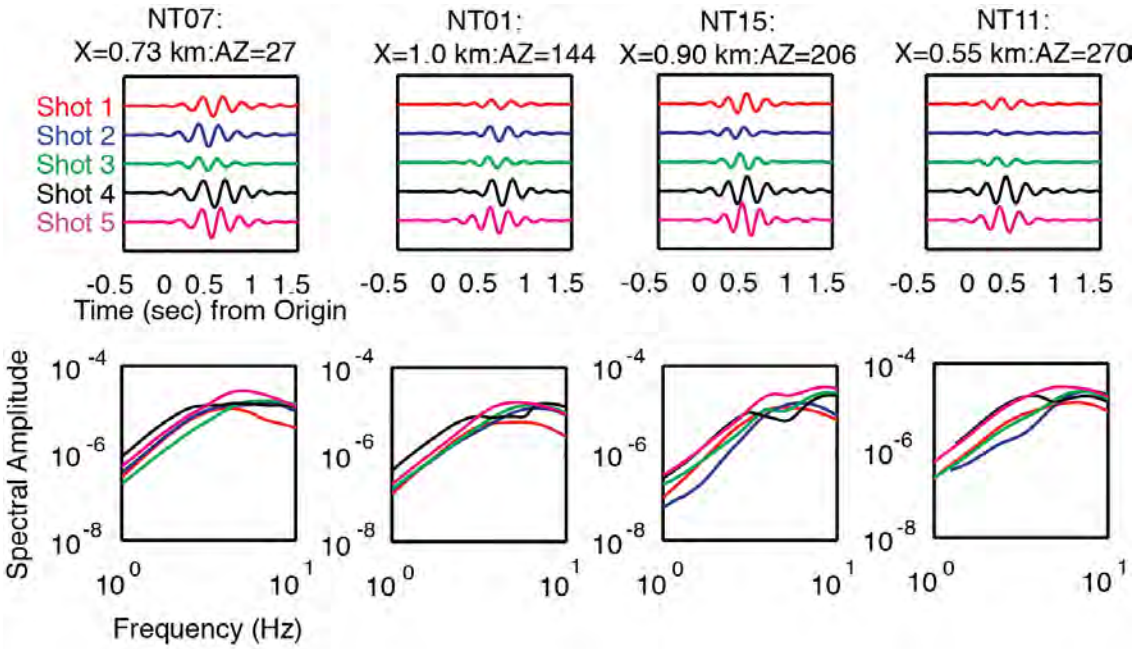

Figure 9. (Top) Near-source 1-5 Hz *Rg* recorded from the NEDE explosions at four near-source (< 1km) vertical-component stations. (Bottom) Displacement spectral amplitudes for *Rg* are also shown.

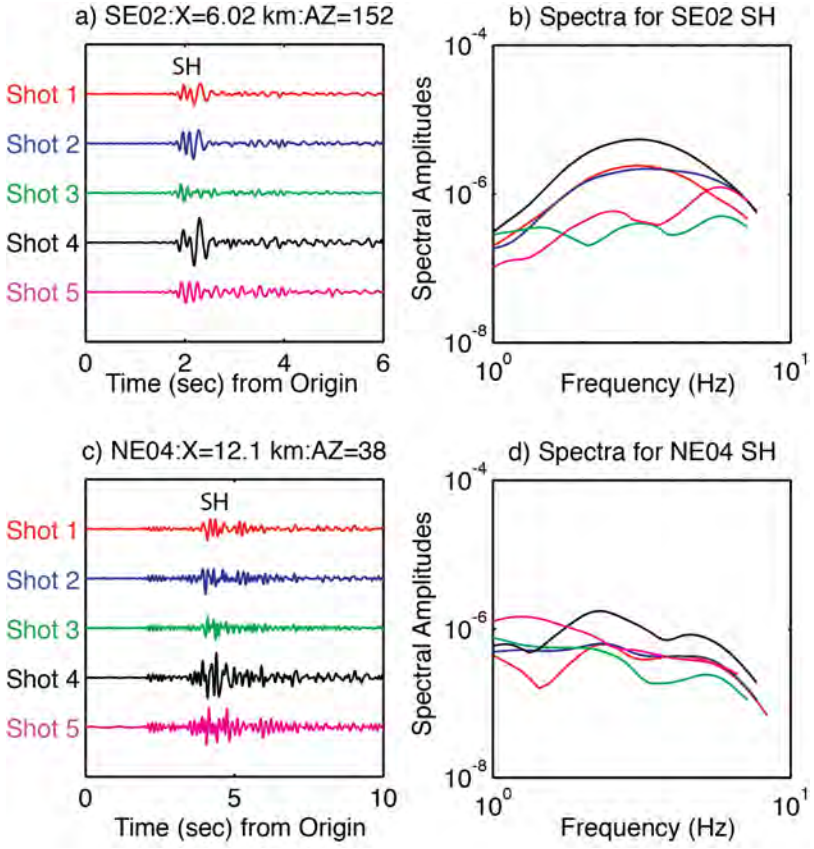

Figure 10. Near-source 1-10 Hz Love waves recorded from the NEDE explosions on transverse components of stations deployed 6 km southeast (top) and 12 km northeast (bottom) of the test site. (Right) Displacement spectral amplitudes for the Love waves.

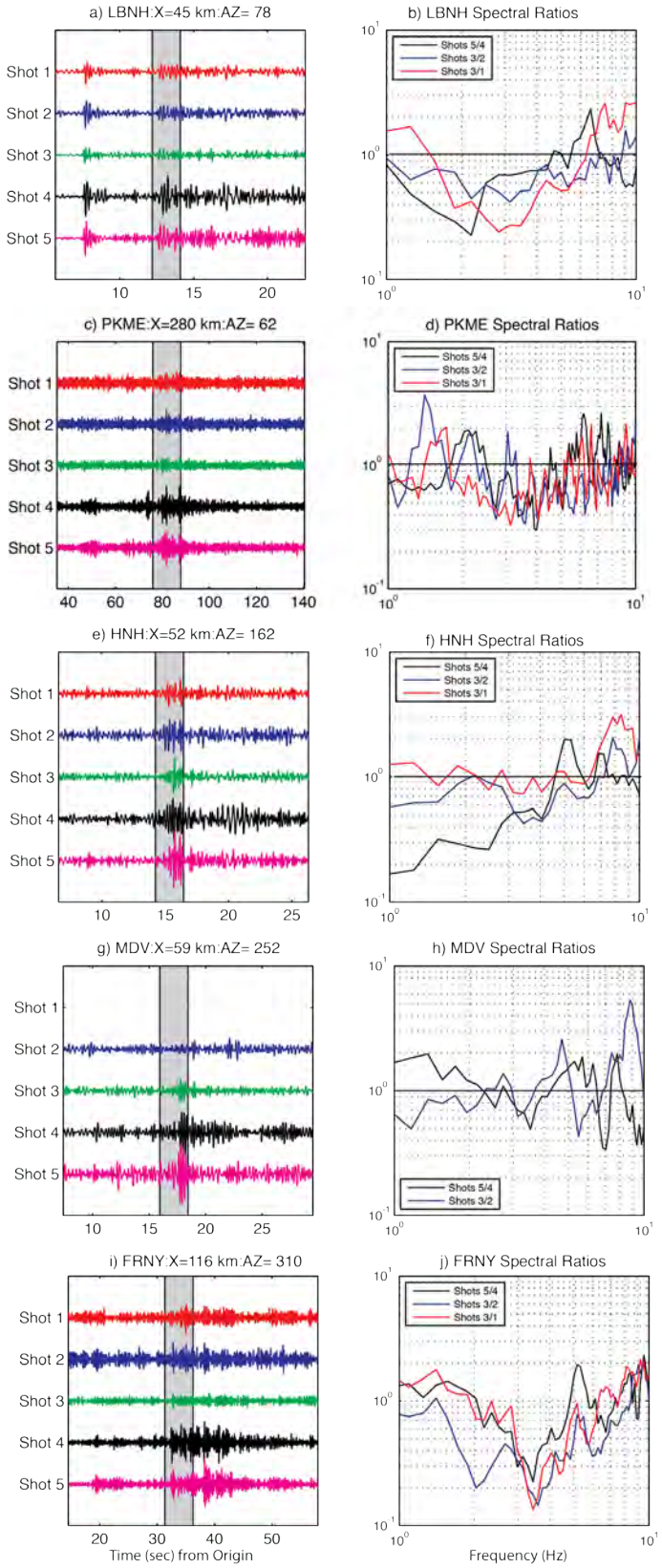

Figure 11. Seismic data and *Lg* spectral ratios for permanent seismic stations in New England that recorded the NEDE shots.

CONCLUSIONS AND RECOMMENDATIONS

New England Research has quantified much of the observed damage from the NEDE blasts. Pre- and post-shot cores show that after the blast, the rock near the shot point had decreased density, increased porosity, higher permeabilities, lower resitivities, and seismic velocity reductions on the order of 20%. The damage region is non-spherical with enhanced damage occurring in the horizontal plane of the explosives emplacement, and could possibly be related to the cylindrical shape of the charges. The entire geometry of the damage zone has not been determined; further investigations in the 2011 field season will focus on this issue. As illustrated in the upper right schematic in Figure 4, one interpretation of the data is an elliptical shape of the damage in plan view. Furthermore, it appears that the damage extends further parallel to the rift plane than normal to it. Coring additional holes perpendicular to the rift will address this issue, and further define the three dimensional nature of blast induced damage. The compilation of these observations coupled with the larger scale fracture damage suggests that the existing models for damage and the zonation of damage generated by underground explosions needs to be reconsidered. Obviously the incorporation of these data into models for shear wave generation may help explain many of Weston Geophysical Corporation's seismic observations.

REFERENCES

Ashby, M.F. and C. G. Sammis (1990). The damage mechanics of brittle solids in compressions. *Pure Appl. Geophys*. 133 489–521.

Brace, W.F., B.W. Paulding, Jr., and C.H. Scholz (1966). Dilatancy in the fracture of crystalline rocks. *J. Geophys. Res.*, 71 (16): 3939.

Bykovtsev, A.S. (2007). Mathematical description of the explosion source with a system of cracks. Abs. *Seism . Res. Letts.*

Patton, H. J. and S. R. Taylor (2011). The apparent explosion moment: Inferences of volumetric moment due to source medium damage by underground nuclear explosions. *J. Geophys. Res*. 116: B03310, doi:10.1029/2010JB007937

Mueller, R. A. and J. R. Murphy (1971). Seismic characteristics of underground nulear detonations: Part I, Seismic scaling law of underground detonations, *Bull Seismol. Soc. Am*., 61: 1675.

Nasseri, M.H.B., and Mohanty, B. (2008). Fracture toughness anisotropy in granitic rocks, *International Journal of Rock Mechanics and Mining Sciences*, 45:167–193.

O'Connell, R. and B. Budiansky (1974). Seismic velocities and in dry and saturated cracked solids. *J. Geophys. Res.*. 70: 5649–5656.

Richter, D. A. (1987). Barre granite quarries, Barre, Vermont, *Geological Society of America Centennial Field Guide*, Northeastern Section.

Sammis, C. (2003). Scaling laws for secondary seismic radiation generated by fracture damage, in *Proceedings of the 25th Seismic Research Review*, LA-UR-03-6029, Vol. 1, pp. 450–455.

Scholz, C. H., (1968). Microfracturing and the inelastic deformation of rock in compression, *J. Geophys. Res.*, 73 (4): 1417.

Short, N. M. (1966). Effects of shock pressures from a nuclear explosion on mechanical and optical properties of granodiorite, *J. Geophys. Res.*, Vol. 71, No. 4: 1195–1215.